Chemical Science

EDGE ARTICLE

View Article Online
View Journal | View Issue

Cite this: *Chem. Sci.*, 2016, **7**, 2066

Discovery and mechanistic study of a photocatalytic indoline dehydrogenation for the synthesis of elbasvir†

Hatice G. Yayla,[a] Feng Peng,[b] Ian K. Mangion,[b] Mark McLaughlin,[b] Louis-Charles Campeau,[b] Ian W. Davies,[b] Daniel A. DiRocco*[b] and Robert R. Knowles*[a]

Received 5th September 2015
Accepted 27th November 2015

DOI: 10.1039/c5sc03350k

www.rsc.org/chemicalscience

Elbasvir is a potent NS5A antagonist for the treatment of chronic hepatitis C. A seemingly trivial indoline oxidation en route to the target compound was complicated by epimerization of a stereogenic hemiaminal center under most standard oxidation conditions. To address this issue, a novel visible light photoredox process for indoline oxidation was developed involving an iridium photosensitizer and environmentally-benign perester oxidant. The reaction was discovered through a high-throughput experimentation campaign and the optimized process was demonstrated on 100 g scale in flow to afford a key intermediate towards the target compound. A battery of kinetic, electrochemical, and spectroscopic studies of this process indicates a radical chain mechanism of dehydrogenation involving selective HAT from the substrate by an alkoxy radicals. Notably, isotope effects were used to validate the chain mechanism when quantum yield data proved ambiguous.

Introduction

More than 150 million people worldwide are infected with the hepatitis C virus (HCV), the leading cause of liver disease and liver transplantations.[1] It is estimated that as many as five million of these people are co-infected with the human immunodeficiency virus (HIV), which typically leads to higher viral loads and results in accelerated disease progression.[2] With limited treatment options for co-infected patients, HCV has become a leading cause of death for HIV patients. Elbasvir, an inhibitor of the HCV NS5A protein (Fig. 1), administered in combination with grazoprevir, an HCV protease inhibitor, has been clinically studied as a highly efficacious, and well tolerated oral regimen for the treatment of HCV infection, including patients with HIV co-infection (Fig. 1). During our development of a synthetic route to elbasvir, a seemingly trivial oxidation of chiral hemiaminal ether **1** to indole **2** proved capricious due to facile epimerization of the hemiaminal stereocenter.[3,4] Following extensive screening, $KMnO_4$ was found to be the only oxidant capable of converting **1** to **2** without loss of enantiopurity (Fig. 1).

Although $KMnO_4$ is an effective oxidant for this transformation, subsequent generation of MnO_2 as a by-product complicates isolation and is environmentally unsustainable for large-scale production. In the pursuit of an alternative method that would circumvent the use of stoichiometric metal oxidants, we elected to investigate the potential efficacy of a redox catalyst that could be turned over with a benign terminal oxidant. Visible-light photoredox catalysis[5] has recently been shown to enable a variety of oxidative, reductive and redox neutral

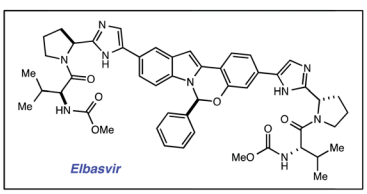

Entry	Oxidant	Solvent	Temp (°C)	Conv (%)	ee (%)
1	$KMnO_4$/$NaHCO_3$	DMA	25	100	99
2	DDQ	PhCl	25	100	90
3	DDQ	CH_2Cl_2	25	100	60
4	$Mn(OAc)_3$/bpy/*t*BuOOH	CH_2Cl_2	50	95	20

Fig. 1 Permanganate-mediated dehydrogenation in the synthesis of elbasvir.

[a]*Department of Chemistry, Princeton University, Princeton, New Jersey 08544, USA. E-mail: rknowles@princeton.edu*

[b]*Department of Process Chemistry, Merck & Co., Inc. Rahway, New Jersey 07065, USA. E-mail: daniel.dirocco@merck.com*

† Electronic supplementary information (ESI) available: Detailed experimental procedures and characterization data for all new compounds. See DOI: 10.1039/c5sc03350k

processes under mild conditions.[6,7] Based on these findings, we elected to explore the viability of a photocatalytic process for the dehydrogenation of **1**. Herein we describe the outcome of these studies and report a novel and scalable catalytic system for the oxidation of **1**. A detailed mechanistic investigation established that indoline oxidation occurs through a radical chain process. Key evidence for the chain process was obtained through the combination of reaction progress kinetic analysis (RPKA) and kinetic isotope effects. We anticipate this protocol will prove useful for elucidating chain processes in photoredox reactions where quantum yield data alone was inconclusive. The results of these studies are described herein.

Results and discussion

Reaction discovery and optimization

High-throughput experimentation was utilized to evaluate a series of photocatalysts and benign terminal oxidants for the dehydrogenation of **1** (Fig. 2). An initial round of experimentation identified both nitromethane and *tert*-butylperacetate (*t*BPA) as competent stoichiometric oxidants, with the most active catalyst identified as the heteroleptic Ir^{III} complex [Ir(dF-CF_3-ppy)$_2$(dtbpy)](PF_6) (Fig. 2, D7, F7). The modest yields in our screening efforts are attributable to post-reaction decomposition, which can be minimized by shortening reaction duration. We and others have previously shown that peresters can be used as efficient electron acceptors in photoredox-catalyzed processes.[8] Moreover, their ease of handling, high availability, low cost and benign decomposition products make them suitable for large-scale manufacturing.[9] As a result, we elected to move forward with perester-based systems for further optimization.

Many photocatalytic processes are rate-limited by the light flux of the reactor; as such, a flow reactor can be used to increase the surface area of the solution and thereby increase light flux and reaction rate.[10–16] A series of experiments were performed in a simple flow reactor, built according to the basic design principles of Booker-Milburn using 440 nm LEDs as the light source.[17] Residence times (τ) between 30 and 60 minutes led to full conversion at catalyst loadings as low as 0.1 mol% using *tert*-butylperbenzoate (*t*BPB) as the oxidant (Table 1, entries 1–2). It was shown that *t*BPA requires a longer τ and leads to more significant erosion of enantiopurity in product **2** (Table 1, entry 3 *vs.* entry 4). Slight erosion of optical purity is observed at higher temperatures (Table 1, entries 5–6); however, maintaining the reactor jacket temperature below 0 °C provided consistently high enantiopurity (Table 1, entries 7, 1). This process was demonstrated on a lab scale at a throughput of 0.04 mol h^{-1} (τ = 60 min). After 5 h, ~100 grams was processed and isolated by direct crystallization upon the addition of water, providing the desired indole in 85% isolated yield and 99.8% ee (Table 1, entry 8).[18] Notably, the photo-mediated reaction compares favorably to the use of permanganate from a process perspective, as the simple workup and direct crystallization of the product from the reaction media results in >60% decrease in the process mass intensity for the step.[19]

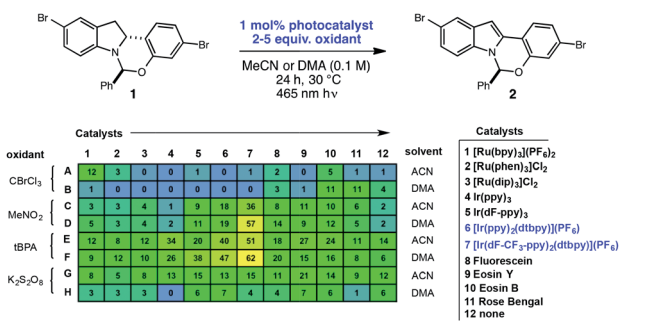

Fig. 2 Identification of a photoredox-mediated dehydrogenation *via* high-throughput experimentation. Reactions performed on 2.5 μmol scale using 465 nm LEDs. Numbers in table refer to assay yields based on HPLC analysis with an internal standard.

Mechanism

With these optimized photocatalytic conditions in hand, we sought to better understand the mechanism of oxidation. A significant challenge in the development of this indoline dehydrogenation was the lability of the hemiaminal stereocenter of **1**, which readily epimerizes with many common oxidants such as 2,3-dichloro-5,6-dicyanobenzoquinone (DDQ), tetracyanoethylene and $Mn(OAc)_3$. A likely pathway for epimerization with single-electron oxidants involves the formation of the radical cation **3**, which could undergo reversible β-scission and erode the stereochemical integrity of the hemiaminal center (Fig. 3).

Given that both the $KMnO_4$ and the photoredox/perester systems led to retention of enantiopurity, we questioned whether there was a fundamental connection between the operative mechanisms of these reactions. Specifically, it is well documented that $KMnO_4$ can act as a hydrogen atom abstractor for benzylic C–H bonds.[20] We therefore postulated that the $KMnO_4$ oxidation may proceed *via* the formation of α-amino radical **6** rather than radical cation **3**. We anticipated that the

Table 1 Optimization of the photoredox indoline oxidation in a 440 nm flow reactor

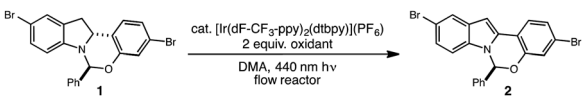

Entry	[**1**]/M	Cat. loading	Oxidant	*t*/min	T[a]/°C	Yield[b] (%)	ee[c] (%)
1	0.5	0.1 mol%	*t*BPB	60	−10	94	99.7
2	0.5	0.1 mol%	*t*BPB	30	0	93	99.9
3	0.4	0.2 mol%	*t*BPB	45	0	90	99.5
4	0.4	0.2 mol%	*t*BPA	90	0	89	99.1
5	0.2	0.5 mol%	*t*BPB	60	25	84	96.7
6	0.2	0.2 mol%	*t*BPA	120	25	88	95.0
7	0.4	0.2 mol%	*t*BPB	45	−10	86	99.8
8	0.5	0.1 mol%	*t*BPB	60	−5	85[d]	99.8

[a] Refers to jacket temperature of reactor. [b] Assay yield based on volumetric HPLC analysis. [c] Enantiomeric excess determined by chiral HPLC analysis. [d] Isolated yield on 100 g scale.

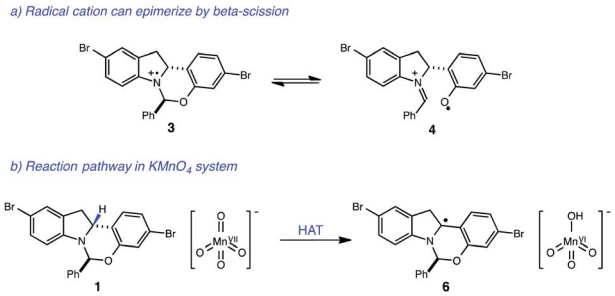

Fig. 3 (a) Proposed pathway for epimerization of starting material. (b) Proposed mechanism for $KMnO_4$-mediated oxidation of indoline core.

hemiaminal stereocenter of intermediate **6** would be configurationally stable, providing a rationale for retention of enantiopurity. Consistent with this view, oxidation of labeled indoline **1b** is markedly slower, suggestive of a rate-determining C–H abstraction step (Fig. 4). Furthermore, isotopologue **1a** performed identically to the original substrate **1** with no loss of either the deuterium label or of optical purity, consistent with the proposal above.

Extending this line of thinking, we reasoned that indoline oxidation using the photoredox/perester system may also proceed *via* a hydrogen atom transfer (HAT) process. Specifically, one-electron reduction of the perester results in O–O bond fragmentation to form an alkoxy radical and carboxylate anion.[21–23] Alkoxy radicals are classical H-atom abstractors, known to readily abstract weak C–H bonds.[24,25] Therefore, hydrogen atom transfer from **1** to the *t*BuO$^{\bullet}$ radical formed upon reduction of *t*BPB would also furnish radical intermediate **6**, identical to the presumed intermediate generated in permanganate oxidations (Fig. 5). Additionally, we wondered whether it was possible for *t*BuO$^{\bullet}$ radicals to initiate a radical chain process wherein HAT from **1** is a propagation step, as outlined in Fig. 6. In recent years, several examples of photoredox catalysts acting as radical chain initiators have appeared in the literature, most notably in the recent work of Yoon.[26–29] In the following sections, our efforts to validate the proposed mechanism and evaluate each elementary step in this reaction sequence are described.

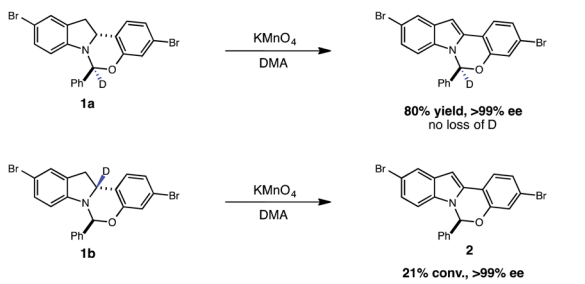

Fig. 4 Isotope-dependence of indoline oxidation with potassium permanganate.

Fig. 5 Proposed indoline oxidation pathway in the perester/photoredox oxidation.

A. Kinetic studies and quantum yield determination. First, the kinetic order of reagents was investigated using Blackmond's reaction progress kinetic analysis (RPKA).[30] Indoline concentration was monitored as a function of time and fit to a polynomial. Taking the derivative of this function provides reaction rate data, which was plotted against indoline concentration to produce a graphical rate equation (see ESI†). Using Blackmond's different excess protocol, we found that the reaction exhibited a first-order kinetic dependence on both indoline and perester concentrations. Moreover, across a wide range of loadings, the reaction is essentially zero-order with respect to the Ir catalyst concentration, consistent with a photon-limited process.[31]

Using this kinetic assay, the quantum yield of indoline oxidation was evaluated. Quantum yields that exceed 1 are often taken as evidence for a radical chain pathway. The quantum yield at any point in the reaction can be defined as the ratio between reaction rate (M s^{-1}) and photon flux (Einsteins L^{-1} s^{-1}).[32] The photon flux at 402 nm through our reactor was assessed to be 2.5×10^5 Einsteins L^{-1} s^{-1}, using potassium ferrioxolate as a chemical actinometer.[33] The wavelength of the emission band for the LEDs was determined (402 nm) using a UVN-SR fiber optic spectrometer.[34] Quantum yield information across the entire range of conversion was then obtained by plotting the ratio of this rate data to photon flux *versus* indoline concentration (Fig. 7). At the outset of the reaction, the quantum yield is ~2 and then decreases as the reaction progresses.[35] While this finding is consistent with a radical chain mechanism, it is not unequivocal evidence. Specifically, non-chain photocatalytic pathways that generate two reactive intermediates from a single excitation event may also produce two equivalents of product, assuming perfect quantum efficiency. To distinguish between these possibilities we turned to the kinetic isotope effect studies described below.

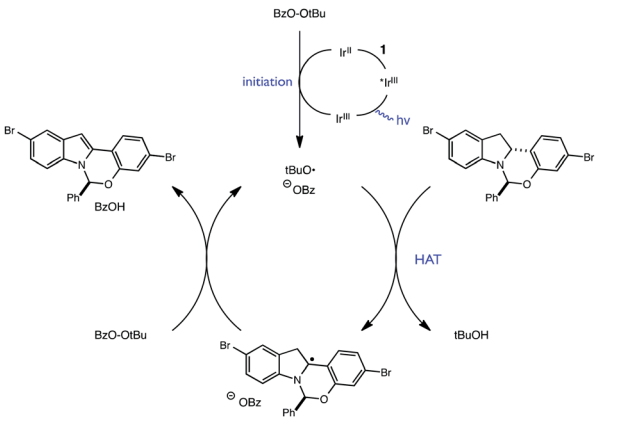

Fig. 6 Proposed chain mechanism.

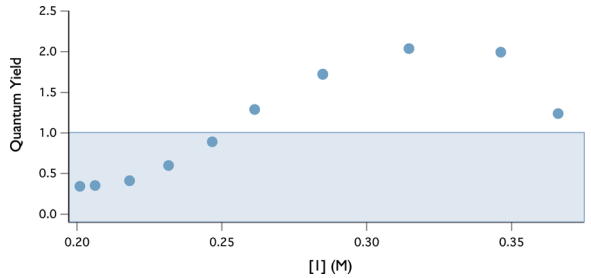

Fig. 7 Quantum yield as a function of reaction progress using 0.1 mol% [Ir(dF-CF_3-ppy)$_2$(dtbpy)](PF_6), 2 equiv. *t*BPB, 1 equiv. **1** in DMA.

B. Isotope effects. To further evaluate the proposed chain mechanism in Fig. 6, we studied a series of direct rate and intermolecular competition kinetic isotope effects (KIEs) using labeled compounds **1** and **1b** (Fig. 8). We anticipated that in a chain process the outcomes of these two experiments would differ characteristically from those expected for a reaction proceeding through a closed catalytic cycle. Specifically, direct rate KIEs, which correspond to the ratio of measured rates for each independent isotopologue, report on the isotopic sensitivities for all of the elementary steps that contribute to the overall reaction rate.[36] Typically, rate laws for chain processes include terms for the initiation, propagation, and termination steps.[37,38] As such, the isotopic sensitivities for all of these elementary steps will be captured in the direct rate KIE. Importantly, the relative contributions of these steps to the overall rate are likely to change over the course of the chain reaction as the concentrations of the reactants decrease, causing the KIE to vary as a function of reaction progress. In contrast, the intermolecular competition KIE (wherein a 1 : 1 mixture of isotopologues react together in the same reaction flask)[39] in a radical chain will reflect almost exclusively on the selectivity for H/D cleavage in the propagation steps, through which the majority of the starting material is consumed. By extension, as the slower steps such as initiation and termination contribute minimally towards the overall degree of starting material consumption, their impact on the intermolecular KIE is expected to be minimal. Moreover, assuming a constant mechanism of C–H/D cleavage, one would expect the competition KIE to be invariant over the entire course of the reaction.

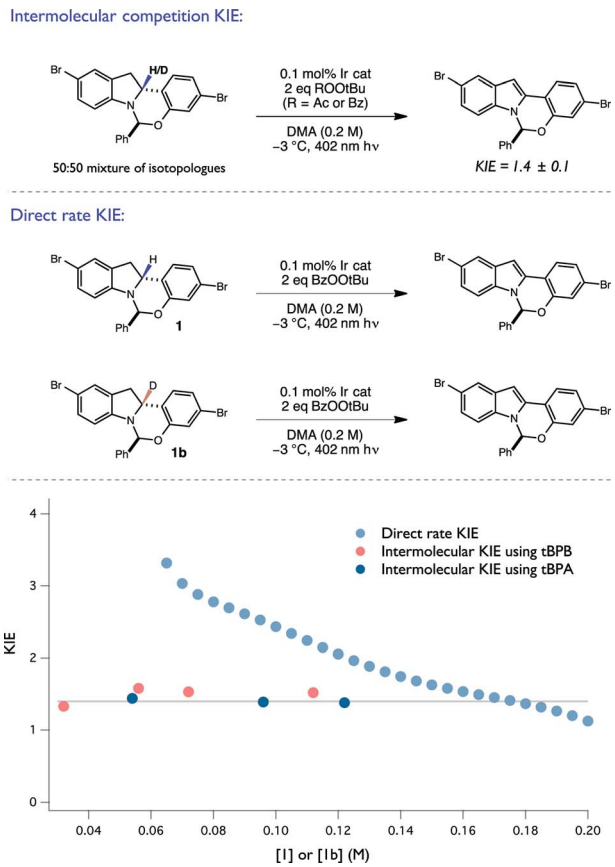

Fig. 8 Summary of KIE experiments with **1b**.

To evaluate the intermolecular competition KIE, a 1 : 1 mixture of **1** and **1b** were oxidized together under standard conditions in the same reaction flask and the degree of isotopic enrichment in the recovered starting material was measured as a function of conversion, resulting in a KIE of 1.4 ± 0.1 (Fig. 8). Importantly, the measured KIE was constant across a large range of conversion, consistent with an invariant mechanism of isotopic discrimination in the C–H/D cleavage event. Moreover, this value of 1.4 is consistent with previously reported KIE values for *t*BuO$^\bullet$ radical-mediated H-atom abstraction from amine α C–H bonds.[25,40] Lastly, competition KIEs using a structurally-distinct perester oxidant, *t*PBA, were also found to provide an identical KIE, consistent with the generation of a common *t*BuO$^\bullet$ radical intermediate when either oxidant is used.

Next, the direct rate KIE was determined using RPKA, wherein two independent reactions, one with protiated and the other with deuterated substrate, were run in parallel. The ratio of the graphical rate equations for the two reactions was then plotted as a function of starting material concentration (Fig. 8). Remarkably, the direct rate KIE was observed to increase markedly as a function of substrate conversion. As the competition KIE results suggest that the selectivity for H/D abstraction remains constant over this range of substrate concentrations, this unusual feature is consistent with a mechanism wherein the relative contributions of any isotopically sensitive initiation and termination steps (*vide infra*) to the overall rate evolve as a function of reaction progress, and by extension with the operation of a radical chain process.

This hypothesis was further bolstered by investigation of H/D KIE at the C-3 position of the indoline. Competition experiments between **1** and **1c** resulted in no measurable KIE at C-3 (k_H/k_D = 0.98 ± 0.02), consistent with an irreversible and selectivity-determining C–H cleavage at C-2 during propagation (Fig. 9). However, when a direct rate KIE for these isotopologues was measured using RPKA (Fig. 9), a substantial inverse KIE (~0.7) was present across a wide range of substrate concentrations. This unusual kinetic feature is also consistent with a radical chain mechanism. Specifically, as the rate constants for termination steps are found in the denominator of chain rate laws, termination steps exhibiting normal KIEs are

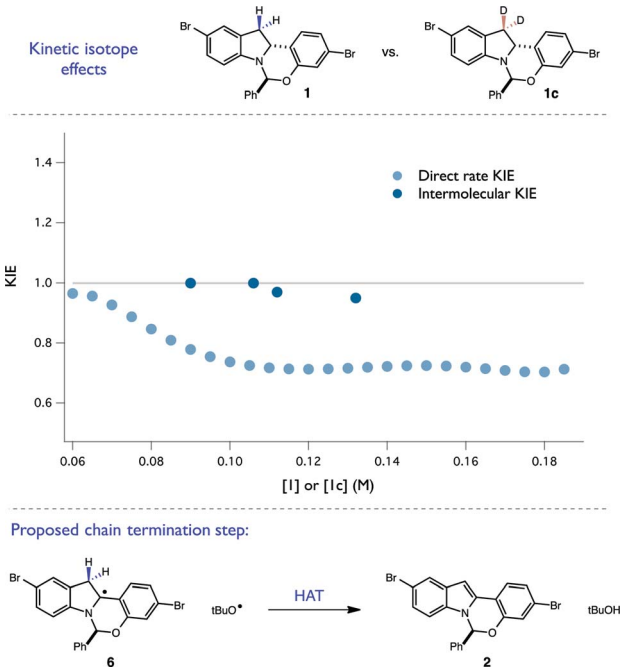

Fig. 9 Summary of KIE experiments with **1c**.

expected to result in overall inverse KIEs. As disproportionation of two radical intermediates is a common mechanism of chain termination, we believe that this inverse KIE is reporting on the isotopic sensitivity of H-atom abstraction from the C-3 position of radical **6** by a *t*BuO• radical. Taken together with the quantum yield findings, we believe that these complex kinetic isotope effects provide a convincing argument for the presence of a radical chain mechanism. More broadly, these experiments present a novel kinetic framework for evaluating radical chain mechanisms involving HAT steps when quantum yield data proves ambiguous. They also demonstrate that caution must be exercised in extrapolating information from direct rate KIE data for chain processes, as the measured values can be highly sensitive to the extent of reaction progress.

Despite the presence of several weak C–H bonds, the KIE studies above suggest that HAT between *t*BuO• radical and indoline **1** to form radical **6** is highly selective for the C-2 position. As the rates of HAT reactions are known to scale with the thermodynamic driving force of the abstraction event, we questioned whether there was a connection between the C–H BDFEs of **6** and the observed site-selectivity.[41,42] Indeed, DFT calculations (UB3LYP/6-311+G(d,p)) (Fig. 10) predict the C-2 methine to be the weakest C–H bond in the molecule, rationalizing the observed site selectivity.

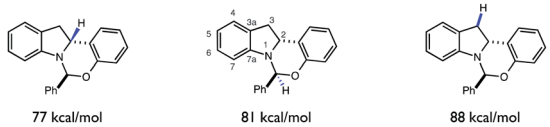

Fig. 10 Uncorrected bond energies for C–H bonds of **1** (UB3LYP/6-311+g(d,p)).

C. Photocatalyst acts as a radical chain initiator through ET. With this knowledge in hand, we next investigated the chain initiation sequence (Fig. 6). Upon irradiation, the Ir complex undergoes a metal-to-ligand charge transfer event and fast intersystem crossing to generate a long-lived triplet excited state that can engage in either electron or energy transfer processes with substrates in solution.[43] Stern–Volmer luminescence quenching studies revealed that the perester *t*BPB does not quench the excited state Ir(III) complex, ruling out direct electron transfer or sensitized homolysis as the source of chain initiation.[44] Rather, we expected that photoexcited Ir catalyst ($^*E_{1/2}(Ir^{III*/II}) = 0.86$ V *vs.* Fc/Fc$^+$ in DMA) might oxidize a sacrificial amount of indoline substrate **1** ($E_p = 0.67$ V *vs.* Fc/Fc$^+$ in DMA), furnishing the reduced state Ir^{II} and the indoline radical cation. Indeed, luminescence quenching studies revealed that this electron transfer readily proceeds with a Stern–Volmer constant (K_{SV}) of 460 M^{-1} in DMA (Fig. 11).[45] The newly formed Ir^{II} complex ($E_{1/2}(Ir^{II/III}) = -1.72$ V *vs.* Fc/Fc$^+$ in DMA) is a strong reductant and is proposed to reduce the perester, *t*BPB ($E_p = -1.91$ V *vs.* Fc/Fc$^+$ in DMA) or *t*BPA ($E_p = -2.00$ V *vs.* Fc/Fc$^+$ in DMA), and form the chain carrying *t*BuO• radical. Additionally, the acidic C–H bonds of the indoline radical cation **3** may also be deprotonated to form radical **6**, which can also propagate the chain. Notably, as an isotopically sensitive initiation step, this process has the potential to impact the magnitude of the direct rate KIE.

While Stern–Volmer studies are routinely employed to evaluate the rates of excited-state electron transfer events, kinetic evaluation of thermal electron transfers between ground state redox partners is more challenging. We were, nonetheless, able to obtain evidence for the viability of the perester reduction by Ir^{II} *via* cyclic voltammetry. Specifically, voltammograms of the Ir catalyst alone exhibit a reversible peak ($E_{1/2} = -1.72$ V *vs.* Fc) for the Ir$^{II/III}$ couple (Fig. 12). However, upon addition of perester, the Ir$^{II/III}$ couple becomes irreversible and a large catalytic wave is observed (Fig. 12). These peak features can be attributed to the reduction of Ir^{III} on the surface of the electrode to form Ir^{II}, followed by reduction of a perester molecule in solution by the

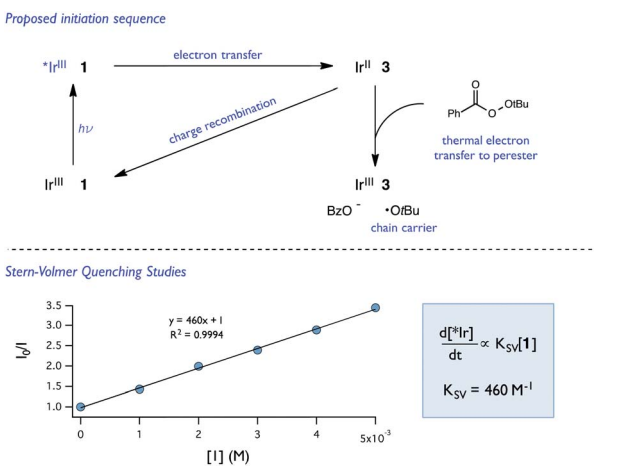

Fig. 11 Proposed initiation sequence and Stern–Volmer quenching studies of **1** and [Ir(dF-CF$_3$-ppy)$_2$(dtbpy)](PF$_6$).

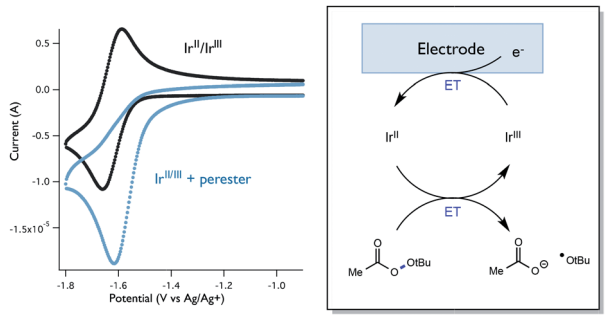

Fig. 12 Voltammetric evidence for catalytic perester reduction by Ir^{II}.

nascent Ir^{II} complex. The resulting Ir^{III} species continues to cycle on the electrode in this fashion, giving rise to the observed catalytic current. The observation of a catalytic wave secures the viability of this elementary step and suggests that it can be plausibly incorporated into the photocatalytic mechanism. While this experimental technique is commonly used to evaluate charge transfer steps in homogeneous electrocatalysis,[46,47] it has, to our knowledge, not been used as a means to study thermal electron transfers in the contemporary synthetic photoredox literature. We anticipate that this simple framework will become a general and useful approach to examine 'dark' electron transfers with reduced and oxidized forms of photocatalysts.

D. Radical propagation *via* perester reduction. Lastly, to perpetuate the radical chain, radical **6** must be competent to activate a second equivalent of the perester and regenerate the chain carrying *t*BuO$^{\bullet}$ radical (see Fig. 6). While classical mechanisms for such processes invoke direct electron transfer, it was found that radical **6** is weakly reducing (by DFT: $E_{1/2}(\mathbf{6}) = -1.07$ V *vs.* Fc/Fc^{+} in MeCN)[48,49] and is unlikely, on thermochemical grounds, to serve as an efficient electron donor to the perester ($E_p = -1.91$ V *vs.* Fc/Fc^{+} in DMA). In light of this, a multisite PCET pathway was considered, wherein radical **6** and benzoic acid act jointly as an electron and proton source for perester reduction.[8a,21] However, voltammetric studies indicate that addition of exogenous benzoic acid does not measurably change the redox potential of perester in DMA, nor does it increase the rate of the reaction (see ESI†). While these findings argue against a PCET process mediated by benzoic acid, it is worth noting that voltammetric measurements made in the presence of stronger acids such as TFA indicated a significant modulation of the perester potential, consistent with a PCET pathway for stronger acids (see ESI†). We also considered a direct H-atom transfer pathway from C-3 of **6** to the perester followed by O–O bond cleavage, which has previously been invoked by Denisov in related peroxide activations and has a large thermodynamic driving force.[41,42,50] However, the direct rate KIE studies outlined above argue against a C-3 HAT being involved in chain propagation. Having ruled out these traditional possibilities, we note that it may also be possible that *t*BuO$^{\bullet}$ radical regeneration occurs *via* a benzoyl transfer from the perester to **6**, followed by subsequent elimination of benzoic acid. However, we have never observed the benzoylated intermediate that would be produced in such a process. As such, the exact nature of the perester activation step remains unclear, though we note that similar questions often surround propagation steps in related Minisci reactions involving peroxide oxidants and weakly reducing radical intermediates.

Conclusions

Herein we have reported the discovery and study of a photoredox-mediated indoline dehydrogenation for the synthesis of elbasvir. Multi-parallel experimentation identified the visible-light photoredox catalyst $[Ir(dF\text{-}CF_3\text{-}ppy)_2(dtbpy)](PF_6)$ and the environmentally-benign oxidant *tert*-butylperbenzoate as the optimal catalyst/oxidant combination, forming the product in high yields with no loss of optical purity. Using a flow reactor, ~100 g of indoline substrate could be processed in just a few hours, providing one of the first demonstrations of photoredox catalysis in the production of a pharmaceutical intermediate. We anticipate that this demonstration will provide further support for the notion that contemporary photoredox catalysis can be carried out efficiently on process-relevant scales.

A detailed mechanistic investigation revealed that this photocatalytic indoline oxidation occurs through a chain process involving a selective and irreversible hydrogen atom abstraction from the C-2 position of **1** by an alkoxy radical. This finding rationalizes the ability of these photocatalytic conditions to maintain the stereochemical integrity of the hemiaminal ether stereocenter, which readily epimerizes using most other oxidation protocols. Evidence for a chain process was secured through a series of complex kinetic isotope studies enabled by reaction progress kinetic analysis and quantum yield experiments. Notably, we expect that this collection of KIE experiments may serve as a general kinetic framework for investigating and elucidating chain mechanisms in situations where quantum yield data proves ambiguous. Additionally, we employed voltammetric techniques to demonstrate the kinetic feasibility of a modestly endergonic thermal electron transfer event between the reduced ground state of the Ir photocatalyst and the perester substrate. We anticipate that this simple protocol will become a general and useful approach to examine 'dark' electron transfers with reduced and oxidized photocatalysts. Taken all together, these studies provide useful new tools for studying the mechanisms of photoredox processes relevant to organic synthesis, and in particular for distinguishing between chain and non-chain processes where more classical methods fail.

Acknowledgements

Barry Rand and Tae-Wook Koh are gratefully acknowledged for assisting with measurement of LED emission spectra. We thank Donald V. Conway (Merck) and Michael K. Wismer (Merck) for design and fabrication of the flow reactor. We also thank Yi Ning Ji Chen for helpful discussions on RPKA. R. R. K. is a Fellow of the Alfred P. Sloan Foundation. We are also thank Lotus Separations for purification of the deuterated compounds **1b** and **1c**.

Notes and references

1 World Health Organization Fact Sheets: Hepatitis C, http://www.who.int/mediacentre/factsheets/fs164/en/, (accessed July 9, 2015).
2 C. A. Coburn, P. T. Meinke, W. Chang, C. M. Fandozzi, D. J. Graham, B. Hu, Q. Huang, S. Kargman, J. Kozlowski, R. Liu, J. A. McCauley, A. A. Nomeir, R. M. Soll, J. P. Vacca, D. Wang, H. Wu, B. Zhong, D. B. Olsen and S. W. Ludmerer, *ChemMedChem*, 2013, **8**, 1930–1940.
3 H. Li, C.-Y. Chen, H. Nguyen, R. Cohen, P. E. Maligres, N. Yasuda, I. Mangion, I. Zavialov, M. Reibarkh and J. Y. L. Chung, *J. Org. Chem.*, 2014, **79**, 8533–8540.
4 I. K. Mangion, C.-Y. Chen, H. Li, P. Maligres, Y. Chen, M. Christensen, R. Cohen, I. Jeon, A. Klapars, S. Krska, H. Nguyen, R. A. Reamer, B. D. Sherry and I. Zavialov, *Org. Lett.*, 2014, **16**, 2310–2313.
5 For reviews on photoredox catalysis: (*a*) T. P. Yoon, M. A. Ischay and J. Du, *Nat. Chem.*, 2010, **2**, 527–532; (*b*) J. M. R. Narayanam and C. R. J. Stephenson, *Chem. Soc. Rev.*, 2011, **40**, 102–113; (*c*) J. W. Tucker and C. R. J. Stephenson, *J. Org. Chem.*, 2012, **77**, 1617–1622; (*d*) C. K. Prier, D. A. Rankic and D. W. C. MacMillan, *Chem. Rev.*, 2013, **113**, 5322–5363; (*e*) M. Reckenthäler and A. G. Griesbeck, *Adv. Synth. Catal.*, 2013, **355**, 2727–2744.
6 (*a*) D. A. Nicewicz and D. W. C. MacMillan, *Science*, 2008, **322**, 77–80; (*b*) M. A. Ischay, M. E. Anzovino, J. Du and T. P. Yoon, *J. Am. Chem. Soc.*, 2008, **130**, 12886–12887; (*c*) J. Du and T. P. Yoon, *J. Am. Chem. Soc.*, 2009, **131**, 14604–14605; (*d*) J. M. R. Narayanam, J. W. Tucker and C. R. J. J. Stephenson, *J. Am. Chem. Soc.*, 2009, **131**, 8756–8757; (*e*) M. Neumann, S. Füldner, B. König and K. Zeitler, *Angew. Chem., Int. Ed.*, 2011, **50**, 951–954; (*f*) A. McNally, C. K. Prier and D. W. C. MacMillan, *Science*, 2011, **334**, 1114–1117; (*g*) M. Rueping, C. Vila, R. M. Koenigs, K. Poscharny and D. C. Fabry, *Chem. Commun.*, 2011, **47**, 2360–2362; (*h*) D. S. Hamilton and D. A. Nicewicz, *J. Am. Chem. Soc.*, 2012, **134**, 18577–18580; (*i*) D. A. DiRocco and T. Rovis, *J. Am. Chem. Soc.*, 2012, **134**, 8094–8097; (*j*) K. T. Tarantino, P. Liu and R. R. Knowles, *J. Am. Chem. Soc.*, 2013, **135**, 10022–10025; (*k*) H. Huo, X. Shen, C. Wang, L. Zhang, P. Rose, L.-A. Chen, K. Harms, M. Marsch, G. Hilt and E. Meggers, *Nature*, 2014, **515**, 100–103; (*l*) C. Cassani, G. Bergonzini and C.-J. Wallentin, *Org. Lett.*, 2014, **16**, 4228–4231.
7 For a recent example of photoredox catalysis applied towards the synthesis of a pharmaceutical target: J. J. Douglas, K. P. Cole and C. R. J. Stephenson, *J. Org. Chem.*, 2014, **79**, 11631–11643.
8 (*a*) D. A. DiRocco, K. Dykstra, S. Krska, P. Vachal, D. V. Conway and M. Tudge, *Angew. Chem., Int. Ed.*, 2014, **53**, 4802–4806; (*b*) H. Rao, P. Wang and C.-J. Li, *Eur. J. Org. Chem.*, 2012, 4580–6507.
9 While all peroxides have an associated risk, the use of low temperatures (<0 °C) and continuous flow conditions minimize this risk. At ~100 °C, *tert*-butylperbenzoate has been shown to undergo exothermic decomposition, see: S.-Y. Cheng, J.-M. Tseng, S.-Y. Lin, J. P. Gupta and C.-M. Shu, *J. Therm. Anal. Calorim.*, 2008, **93**, 121–126.
10 Y. Su, N. J. W. Straathof, V. Hessel and T. Noël, *Chem.–Eur. J.*, 2014, **20**, 10562–10589.
11 J. W. Tucker, Y. Zhang, T. F. Jamison and C. R. J. Stephenson, *Angew. Chem., Int. Ed.*, 2012, **51**, 4144–4147.
12 F. R. Bou-Hamdan and P. H. Seeberger, *Chem. Sci.*, 2012, **3**, 1612–1616.
13 R. S. Andrews, J. J. Becker and M. R. Gagné, *Angew. Chem., Int. Ed.*, 2012, **51**, 4140–4143.
14 Z. J. Garlets, J. D. Nguyen and C. R. J. Stephenson, *Isr. J. Chem.*, 2014, **54**, 351–360.
15 D. Cantillo, O. de Frutos, J. A. Rincón, C. Mateos and C. O. Kappe, *Org. Lett.*, 2014, **16**, 896–899.
16 Z. He, M. Bae, J. Wu and T. F. Jamison, *Angew. Chem., Int. Ed.*, 2014, **53**, 14451–14455.
17 B. D. A. Hook, W. Dohle, P. R. Hirst, M. Pickworth, M. B. Berry and K. I. Booker-Milburn, *J. Org. Chem.*, 2005, **70**, 7558–7564.
18 For another recent report of a large-scale photoredox reaction, see: J. W. Beatty, J. J. Douglas, K. P. Cole and C. R. J. Stephenson, *Nat. Commun.*, 2015, **6**, 7919–6.
19 PMI is a measure of the overall efficiency of the process. It is defined as the ratio between the total mass of reagent input and the total mass of product output. See ESI† for a comparative PMI analysis of both oxidation protocols ($KMnO_4$ *vs.* photoredox oxidation).
20 (*a*) K. A. Garder, L. L. Kuehnert and J. M. Mayer, *Inorg. Chem.*, 1997, **36**, 2069–2078; (*b*) J. M. Mayer, *Acc. Chem. Res.*, 1998, **31**, 441–450.
21 Example of PCET-mediated reductive cleavage of peroxides: C. Costentin, V. Hajj, M. Robert, J.-M. Saveant and C. Tard, *Proc. Natl. Acad. Sci. U. S. A.*, 2011, **108**, 8559–8564.
22 S. Antonello, F. Formaggio, A. Moretto, C. Toniolo and F. Maran, *J. Am. Chem. Soc.*, 2001, **123**, 9577–9584.
23 R. Baron, A. Darchen and D. Hauchard, *Electrochim. Acta*, 2006, **51**, 1336–1341.
24 M. Finn, R. Friedline, N. K. Suleman, C. J. Wohl and J. M. Tanko, *J. Am. Chem. Soc.*, 2004, **126**, 7578–7584.
25 D. Griller, J. A. Howard, P. R. Marriott and J. C. Scaiano, *J. Am. Chem. Soc.*, 1981, **103**, 619–623.
26 M. A. Cismesia and T. P. Yoon, *Chem. Sci.*, 2015, **6**, 5426–5434.
27 For other examples in photoredox catalysis with high reported quantum yields: (*a*) Ł. Woźniak, J. J. Murphy and P. Melchiorre, *J. Am. Chem. Soc.*, 2015, **137**, 5678–5681; (*b*) M. Majek, F. Filace and A. J. V. Wangelin, *Beilstein J. Org. Chem.*, 2014, **10**, 981–989; (*c*) K. Gollnick and A. Schnatterer, *Tetrahedron Lett.*, 1984, **25**, 185–188.
28 For examples in photoredox catalysis where a radical chain mechanism is invoked: (*a*) J. W. Beatty and C. R. J. Stephenson, *Acc. Chem. Res.*, 2015, **48**, 1474–1484; (*b*) L. Ruiz Espelt, E. M. Wiensch and T. P. Yoon, *J. Org. Chem.*, 2013, **78**, 4107–4114; (*c*) M. A. Ischay, M. S. Ament and T. P. Yoon, *Chem. Sci.*, 2012, **3**, 2807–2811; (*d*) S. Lin, M. A. Ischay, C. G. Fry and T. P. Yoon, *J. Am. Chem. Soc.*,

2011, **133**, 19350–19353; (*e*) A. E. Hurtley, M. A. Cismesia, M. A. Ischay and T. P. Yoon, *Tetrahedron*, 2011, **67**, 4442–4448; (*f*) C.-J. Wallentin, J. D. Nguyen, P. Finkbeiner and C. R. J. Stephenson, *J. Am. Chem. Soc.*, 2012, **134**, 8875–8884; (*g*) O. O. Fadeyi, J. J. Mousseau, Y. Feng, C. Allais, P. Nuhant, M. Z. Chen, B. Pierce and R. Robinson, *Org. Lett.*, 2015, **17**, 5756–5759.

29 For an elegant mechanistic study detecting key radical intermediates in a photoredox system, see: N. A. Romero and D. A. Nicewicz, *J. Am. Chem. Soc.*, 2014, **136**, 17024–17035.

30 For perspectives on RPKA, see: (*a*) J. S. Mathew, M. Klussmann, H. Iwamura, F. Valera, A. Futran, E. A. C. Emanuelsson and D. G. Blackmond, *J. Org. Chem.*, 2006, **71**, 4711–4722; (*b*) D. G. Blackmond, *Angew. Chem., Int. Ed.*, 2005, **44**, 4302–4320; (*c*) D. G. Blackmond, *J. Am. Chem. Soc.*, 2015, **137**, 10852–10866. For a recent example using RPKA in photoredox catalysis, see: (*d*) J. J. Devery III, J. J. Douglas, J. D. Nguyen, K. P. Cole, R. A. Flowers II and C. R. J. Stephenson, *Chem. Sci.*, 2015, **6**, 537–541. For recent examples of RPKA used in catalysis, see: (*e*) J. S. Bandar, M. T. Pirnot and S. L. Buchwald, *J. Am. Chem. Soc.*, 2015, **137**, 14812–14818; (*f*) M. Scott, A. Sud, E. Boess and M. Klussmann, *J. Org. Chem.*, 2014, **79**, 12033–12040; (*g*) R. D. Baxter, D. Sale, K. M. Engle, J.-Q. Yu and D. G. Blackmond, *J. Am. Chem. Soc.*, 2012, **134**, 4600–4606; (*h*) K. A. Choquette, D. V. Sadasivam and R. A. Flowers II, *J. Am. Chem. Soc.*, 2011, **133**, 10655–10661; (*i*) J. J. Devery III, J. C. Conrad, D. W. C. MacMillan and R. A. Flowers II, *Angew. Chem., Int. Ed.*, 2010, **49**, 6106–6110; (*j*) S. J. Zuend and E. N. Jacobsen, *J. Am. Chem. Soc.*, 2009, **131**, 15358–15374.

31 Notably, at very low loadings, an induction period emerges. This is likely due to trace inhibitors in solution. Furthermore, a "same excess" experiment was performed to validate that there was no kinetically significant catalyst deactivation occurring under the standard reaction conditions (0.1 mol% Ir). See ESI† for more details.

32 P. Klan and J. Wirz, *Photochemistry of Organic Compounds: From Concepts to Practice*, Wiley, Chichester, UK, 2009, p. 110.

33 (*a*) C. G. Hatchard and C. A. Parker, *Proc. R. Soc. A*, 1956, **235**, 518–536; (*b*) H. J. Kuhn, S. E. Braslavsky and R. Schmidt, *Pure Appl. Chem.*, 2004, **76**, 2105–2146.

34 60% of the photons emitted from the LEDs are emitted are between 397 nm and 407 nm. See ESI† for an emission spectrum of the LEDs used.

35 It should also be noted that as the reaction progresses, the quantum yield eventually drops below 1. This does not necessarily represent a change in mechanism, but rather reflects the decline in reaction rate as starting material is depleted. It is well established that reactions with long chain lengths (>100) can exhibit quantum yields below the classic threshold of 1. For an example, refer to: J. E. Argüello, A. B. Peñéñory and R. A. Rossi, *J. Org. Chem.*, 2000, **65**, 7175–7182.

36 E. M. Simmons and J. F. Hartwig, *Angew. Chem., Int. Ed.*, 2012, **51**, 3066–3072.

37 (*a*) J. K. Kochi, *Free Radicals*, Wiley-Interscience, New York, 1973; (*b*) G. Odian, *Principles of Polymerization*, John Wiley & Sons, Inc., Hoboken, NJ, 4th edn, 1985, ch. 3, p. 198; (*c*) D. Watts, *Dent. Mater.*, 2005, **21**, 27–35.

38 For elegant kinetic studies that showcase the contribution of specific termination step on the overall rate, see: (*a*) C. Walling and V. Kurkov, *J. Am. Chem. Soc.*, 1966, **88**, 4727–4728; (*b*) C. Walling and V. Kurkov, *J. Am. Chem. Soc.*, 1967, **89**, 4895–4901.

39 L. Melander and W. H. Saunders Jr, *Reaction Rates of Isotopic Molecules*, John Wiley and Sons Inc., New York, 1980, p. 95.

40 J. M. Tanko, R. Friedline, N. K. Suleman and N. Castagnoli, *J. Am. Chem. Soc.*, 2001, **123**, 5808–5809.

41 (*a*) J. P. Roth, J. C. Yoder, T.-J. Won and J. M. Mayer, *Science*, 2001, **294**, 2524–2526; (*b*) J. M. Mayer, *Acc. Chem. Res.*, 2011, **44**, 36–46; (*c*) J. M. Mayer, *Annu. Rev. Phys. Chem.*, 2004, **55**, 363–390.

42 M. G. Evans and M. Polanyi, *Trans. Faraday Soc.*, 1938, **34**, 11–24.

43 M. S. Lowry, J. I. Goldsmith, J. D. Slinker, R. Rohl, R. A. Pascal, G. G. Malliaras and S. Bernhard, *Chem. Mater.*, 2005, **17**, 5712–5719.

44 For an example where the Ir photocatalyst sensitizes substrates *via* energy transfer, see: Z. Lu and T. P. Yoon, *Angew. Chem., Int. Ed.*, 2012, **51**, 10329–10332.

45 The presence of a hyperconjugative KIE during one-electron oxidation of 1 was also investigated with a Stern–Volmer luminescence quenching experiment and no significant KIE was observed. For experimental details, refer to the ESI†

46 J.-M. Saveant, *Elements of molecular and biomolecular electrochemistry: An Electrochemical Approach to Electron Transfer Chemistry*, Wiley-Interscience, Hoboken, NJ, 2006, ch. 4.

47 E. S. Rountree, B. D. McCarthy, T. T. Eisenhart and J. L. Dempsey, *Inorg. Chem.*, 2014, **53**, 9983–10002.

48 Y. Fu, L. Liu, H.-Z. Yu, Y.-M. Wang and Q.-X. Guo, *J. Am. Chem. Soc.*, 2005, **127**, 7227–7234.

49 S. J. Konezny, M. D. Doherty, O. R. Luca, R. H. Crabtree, G. L. Soloveichik and V. S. Batista, *J. Phys. Chem. C*, 2012, **116**, 6349–6356.

50 E. T. Denisov, T. G. Denisova and T. S. Pokidova, *Handbook of Free Radical Initiators*. Wiley – Interscience, Hoboken, NJ, 2003, p. 772.